

OBSERVATIONS OF OJ 287 FROM THE GEODETIC VLBI ARCHIVE OF THE WASHINGTON CORRELATOR

C. E. TATEYAMA

Centro de Rádio-Astronomia e Aplicações Espaciais/CRAAE-INPE, Instituto Presbiteriano Mackenzie, Rua da Consolação 896, 01302-000, São Paulo, SP, Brazil

K. A. KINGHAM

U.S. Naval Observatory, Earth Orientation Dept, 3450 Massachusetts Ave, Washington D.C. 20392, USA

P. KAUFMANN

Centro de Rádio-Astronomia e Aplicações Espaciais/CRAAE-Mackenzie, Instituto Presbiteriano Mackenzie, Rua da Consolação 896, 01302-000, São Paulo, SP, Brazil

B. G. PINER

Jet Propulsion Laboratory, California Institute of Technology, MS 238-332, 4800 Oak Grove Dr., Pasadena, CA 91109

L. C. L. BOTTI

Centro de Rádio-Astronomia e Aplicações Espaciais/CRAAE-INPE, Instituto Presbiteriano Mackenzie, Rua da Consolação 896, 01302-000, São Paulo, SP, Brazil

AND

A. M. P. DE LUCENA

ROEN, Rádio Observatório Espacial do Nordeste, CRAAE-INPE, Estrada do Fio, 6000, Eusébio (Fortaleza), CE, Brazil

Draft version September 11, 2018

ABSTRACT

We present 27 geodetic VLBI maps of OJ 287 obtained from the archive of the Washington correlator. The observations presented here were made between 1990 October and 1996 December. During this period a sequence of six superluminal components has been identified. We measured the proper motion of these components to be approximately 0.5 mas yr^{-1} , which is about twice as high as that seen in previous VLBI observations. These results imply a higher component ejection rate than previously observed, in good agreement with the observed occurrences of radio outbursts. We have examined a possible connection between VLBI components and optical flares in the framework of a binary black hole system.

Subject headings: Galaxies: Jets — BL Lacertae objects: individual (OJ 287) — radio continuum: galaxies

1. INTRODUCTION

OJ 287 is a highly variable radio source at $z = 0.306$ (Miller, French, & Hawley 1978; Sitko & Junkkarinen 1985). The nature of the underlying galaxy is not well known; Kinman (1975) and Hutchings et al. (1984) detected a nebulosity that might be a galaxy. The light curve of OJ 287 presents a complex structure, but its most interesting aspect is the series of prominent flares which recur with a period of 12 years (Sillanpää et al. 1988). Recent V-band observations have revealed double-peaked outbursts (Sillanpää et al. 1996; Lehto & Valtonen 1996). To reproduce the cyclic 12 year optical flares, OJ 287 has become the best candidate to harbor a supermassive binary black hole system. Sillanpää et al. (1988) used such a system in which the light variations were related to tidally induced mass flows from the accretion disk into the black hole to explain the periodicity in OJ 287's light curve. The orbit of the secondary black hole was assumed to be coplanar with the accretion disk. Lehto & Valtonen (1996) suggested a binary system model where the primary is surrounded by an accretion disk with a high inclination angle relative to the orbit of the secondary. A major flare would be observed whenever the secondary crossed the disk of the primary. The binary system model of Villata et al. (1998) with two independent relativistic jets and the nodding disk

model of Katz (1997) use a sweeping beam approach to explain the same optical flares.

The radio light curves are dominated by outbursts at irregular intervals of about a year, and modulated by a much longer non-periodic timescale (Usher 1979). Analysis of radio-optical events in OJ 287 has shown correlated activity. Usher (1979) compared events from 1966 to 1978 and proposed that most optical outbursts are synchronous with radio counterparts. Valtaoja, Sillanpää, & Valtaoja (1987) studied isolated flaring events and found that optical variations preceded the radio ones by a few months.

VLBI observations of OJ 287 have been made at 5 GHz (Roberts, Gabuzda, & Wardle 1987; Gabuzda, Wardle, & Roberts 1989), 8 GHz (Vicente, Charlot, & Sol 1996), and 43 and 100 GHz (Tateyama et al. 1996). Superluminal motion was first detected from VLBI polarization data at 5 GHz (Roberts et al. 1987). Previously to this paper, three superluminal knots — named K1, K2 and K3 — have been followed from 1981 to 1988. The observed proper motion of these components corresponds to an apparent superluminal speed between 3.7 and $5.1c$ ($H_0 = 65 \text{ km s}^{-1} \text{ Mpc}^{-1}$, $q_0 = 0.5$). In a single epoch VLBI observation at 8.3 GHz, a new jet component K4 and another polarization component located between the core and K4 named K5 have been added to the list of components of OJ 287 by Gabuzda & Cawthorne (1996). More recently,

Vicente et al. (1996) fitted a helical path with two consecutive loops to the trajectory of component K3.

We present 27 geodetic VLBI maps at 8.3 GHz obtained from the Washington correlator's database. Geodetic VLBI maps have been successfully used for astrophysical studies of compact sources (e.g., Guoqiang, Rönnäng & Bååth 1987; Charlot 1990; Britzen et al. 1994; Vicente et al. 1996). More recently, Piner & Kingham (1998), and Tateyama et al. (1998) have obtained interesting results for a group of EGRET blazars and BL Lac respectively using the Washington VLBI correlator's database.

2. OBSERVATIONS

The VLBI observations used in this paper are from geodetic VLBI data archived at the Washington correlator. These data were obtained from geodetic dual-frequency VLBI experiments (Rogers et al. 1983) carried out by the Naval Observatory (Eubanks et al. 1991), the National Oceanographic and Atmospheric Administration (Carter, Robertson, & MacKay 1985), the Crustal Dynamics Project, and the Space Geodesy Project, (Coates et al. 1985; Smith & Turcotte 1993). The VLBI observations were processed at the Washington VLBI Correlator at the U.S. Naval Observatory (USNO).

All observations were obtained with Mark-III dual-frequency VLBI receivers at both X- and S-band (centered at 8.5 and 2.3 GHz respectively), providing noise temperatures of 70 K - 200 K. X-band consists of 8 individual channels of 2 MHz bandwidth spanning the range 8.2 to 8.9 GHz. All stations were equipped with H-masers as the local frequency standards. Geodetic VLBI data useful for imaging OJ 287 begins to appear in the Washington Correlator archive around 1990. Table 1 lists all observations used in this work: column 1 gives the epochs of the observations, column 2 the names of the experiments, column 3 the antennas participating in the experiments, column 4 the peak brightness of the images, column 5 the interferometric dirty beams, column 6 the position angles of the beams measured from north through east, and the last column the number of scan-baselines in the observations, where the number of scan-baselines is the sum over all the scans of the number of baselines per scan. The dirty beams were about 0.5 - 0.6 mas in size for all maps. We have used a restored circular beam of 0.6 mas on the maps. The dynamic range defined as the ratio of the peak flux per beam to the lowest positive contour in the maps is about 300:1. The total length in which the moving components in OJ 287 can be followed with the geodetic network appears to be limited to radii not much greater than 1.5 mas. This is about half the distance reached by the knots in the 5 GHz VLBI observations made by Roberts et al. (1987) and Gabuzda et al. (1989). Except for CRD96GH (Table 1) where the resulting map is the sum of the experiments CRD96G and CRD96H observed on Sep 19 and Sep 20 of 1996 respectively, all maps were obtained from a single geodetic observation.

The data were coherently averaged to four seconds to determine the visibilities. The data were calibrated and fringed using standard routines from AIPS software package, and the images were produced using the self-calibration procedures (e.g. Pearson & Readhead 1984) of the Caltech Difmap software package.

3. RESULTS

Throughout this paper we assume a standard Friedmann cosmology with $H_0 = 65 \text{ km s}^{-1} \text{ Mpc}^{-1}$ and $q_0 = 0.5$. At the distance of OJ 287 ($z = 0.306$), an angular size of 1 mas corresponds to a linear distance of 4.3 pc. The 8 GHz radio maps are presented in Figure 1. The source shows a core-jet structure, with jet components moving in a westerly direction. Table 2 lists the flux, position, and size of each component obtained by model fitting the observed visibilities with elliptical Gaussian components. Position angle is measured from north through east.

The motion of the components away from the core can be better appreciated by inspecting Figure 2, where the separation of components from the core is plotted against time. The straight lines provide estimates of the presumed zero separation of the components C1 to C6 under the assumption of rectilinear motion at constant velocity. The measured proper motions of the components C1 to C6 are 0.74 ± 0.40 , 0.44 ± 0.05 , 0.52 ± 0.09 , 0.40 ± 0.13 , 0.46 ± 0.05 , and $0.58 \pm 0.07 \text{ mas yr}^{-1}$ respectively, corresponding to an average superluminal speed of approximately $9c$. These values are almost twice as high as those seen in VLBI observations made at 5 GHz by Roberts et al. (1987) and Gabuzda et al. (1989). A similar proper motion has also been obtained by Vicente et al. (1996) for the fastest part of the motion of component K3 (0.4 mas yr^{-1}). The number of components observed over this time range, together with their measured speeds, suggests more frequent ejection of VLBI components than has been previously estimated for this source by Vicente et al. (1996), who concluded that VLBI component ejections occurred at intervals of one-half the orbital period of the putative binary black hole system, or once every six years. The small separation between successive components obtained by Gabuzda & Cawthorne (1996) at 8 GHz and Tateyama et al. (1996) at 43 GHz also suggests a higher ejection rate. We can constrain these results using radio light curves, provided that radio outbursts are connected with VLBI components.

4. DISCUSSION

4.1. Radio Light Curves

Figure 3 shows the optical and radio light curves of OJ 287. The beginning of each radio outburst is indicated by a vertical line. There is a good agreement between the epochs of the radio outbursts and the epochs of zero separation of components C1 to C6 which are 1989.5, 1990.0, 1991.7, 1992.5, 1993.3, and 1995.4 respectively. Only C2 would require a higher proper motion for its zero separation epoch to match with the beginning of the radio outburst around 1990.2. However, we may place the 43 GHz data point a little closer to the core, accounting for a possible frequency-dependent separation between it and the 8 GHz data. Since the 8 GHz measurement of Gabuzda & Cawthorne (1996) is not clearly resolved from the core, it may also be placed closer to the core, resulting in a zero separation epoch for C2 more consistent with the beginning of the outburst.

The zero separation epoch of C1 is estimated from only two points. The point closer to the core was taken from 8 GHz VLBI observations obtained by Gabuzda & Cawthorne (1996). The extrapolation of the fitted motion

TABLE 1
8.4 GHz VLBI OBSERVATIONS OF OJ 287.

Epoch	Name	Antennas	Peak brightness [Jy beam ⁻¹]	Synthesized beam [mas x mas]	Beam angle [deg]	Number of scan-baselines
90 Oct 27	NAPSA	JYEAC	4.9	1.6 x 1.3	39	139
92 Aug 03	IR752	GJREV	2.3	1.8 x 0.7	-19	48
92 Aug 10	IR753	GJREV	2.4	1.0 x 0.7	-15	53
93 Jun 24	NB02	AIWVGT	1.3	1.6 x 0.6	-2	66
93 Dec 10	NB08	GIWTV	1.5	2.5 x 0.5	-10	63
94 Sep 02	NB16	GXAIWTV	1.0	1.5 x 0.6	2	59
94 Dec 13	NE85	FAKWVN	1.0	0.5 x 0.5	-35	63
95 Jan 25	NA91	FAKWV	0.9	0.7 x 0.4	20	22
95 Apr 18	NA103	FAKWVO	0.8	0.9 x 0.6	-21	51
95 Jun 14	NXS6	GAMWOV	0.8	1.1 x 0.7	-29	51
95 Sep 19	NA125	GFAKWNV	1.2	1.3 x 0.6	-4	29
95 Oct 17	NA129	GFAKHLNV	1.4	0.7 x 0.5	17	80
95 Dec 12	NA137	FAKNOV	2.0	0.7 x 0.6	-75	63
96 Mar 05	NA149	FAKNOV	1.2	0.8 x 0.6	-39	62
96 Mar 26	NA152	FAKNOV	1.1	0.8 x 0.6	-34	61
96 Apr 02	NA153	FAKMNV	1.2	0.9 x 0.6	2	67
96 Apr 24	NXS10	GAKNOV	0.9	0.9 x 0.7	-14	22
96 Aug 20	NA173	FAKWNOV	1.1	0.6 x 0.5	15	63
96 Sep 03	NA175	FAKNOV	1.1	0.8 x 0.5	-58	51
96 Sep 17	NA177	FAKNOV	1.1	0.7 x 0.6	-27	69
96 Sep 19	CRD96GH	AKNOV	0.9	0.8 x 0.6	-22	204
96 Oct 01	NA179	FAKNOV	1.2	1.0 x 0.5	-16	68
96 Oct 02	CRD96J	AKNOV	1.0	0.9 x 0.5	-18	98
96 Oct 03	CRD96K	AKNOV	0.9	1.0 x 0.5	-20	79
96 Oct 04	CRD96L	AKNOV	1.0	1.0 x 0.6	-23	91
96 Nov 12	NA185	FAKNOV	1.3	0.6 x 0.4	8	61
96 Dec 10	NA189	FAKNOV	1.1	0.9 x 0.5	-46	62

NOTE.— A = Gilcreek (Alaska, 26 m), C = Hat Creek (California, 26 m), E = Westford (Massachusetts, 18 m), F = Fortaleza (Brazil, 14 m), G = Algotpark (Ontario, 46 m), H = MK-VLBA (Hawaii, 25 m) I = Matera (Italy, 20 m), J = Mojave (California, 12 m), K = Kokee (Hawaii, 20 m), L = NL-VLBA (Iowa, 25 m) M = Miami20 (Florida, 20 m), N = NRAO20 (West Virginia, 20 m), O = Ny Alesund (Norway, 20 m), R = Richmond (Florida, 18 m), T = Onsala (Sweden, 20 m), V = Wettzell (Germany, 20 m), X = Ylow7296 (Northwest Territories, 10 m), Y = Plattville (North Carolina, 5 m), W = NRAO85 (West Virginia, 26 m)

TABLE 2
 MODEL FITS TO OJ 287 AT 8 GHz.

Epoch	Comp.	Flux [Jy]	r [mas]	PA ^a [°]	θ^b [mas]	AR ^c	PA ^d [°]
90 Oct 27	core	4.40	0	...	0.15	0.8	0
	C1	1.21	0.98	-109	0.70	0.8	60
92 Aug 03	core	2.20	0	...	0.19	0.8	80
	C3	0.76	0.51	-98	0.30	0.8	-38
	C2	0.21	1.24	-110	1.10	0.8	5
92 Aug 10	core	2.30	0	...	0.17	0.8	-60
	C3	0.55	0.49	-99	0.30	0.8	-45
	C2	0.27	1.17	-110	0.90	0.7	50
93 Jun 24	core	1.05	0	...	0.15	0.7	0
	C4	0.61	0.39	-89	0.54	0.6	105
	C3	0.23	0.98	-99	1.10	0.7	-70
93 Dec 10	core	1.56	0	...	0.19	1.0	...
	C4	0.54	0.55	-102	0.30	0.7	-10
	C3	0.48	1.19	-85	0.80	0.5	0
94 Sep 02	core	1.25	0	...	0.10	1.0	...
	C5	0.55	0.62	-88	0.40	1.0	...
94 Dec 13	core	0.93	0	...	0.13	0.8	-10
	C5	0.89	0.79	-95	0.80	0.8	90
95 Jan 25	core	0.97	0	...	0.17	0.9	-75
	C5	0.54	0.82	-93	0.70	0.8	-90
95 Apr 18	core	0.76	0	...	0.17	0.8	-80
	C5	0.58	0.98	-90	0.90	0.8	80
95 Jun 14	core	0.83	0	...	0.17	0.7	-41
	C5	0.28	1.06	-99	1.16	0.7	10
95 Sep 19	core	1.26	0	...	0.20	0.8	-50
	C5	0.40	1.13	-96	0.93	0.8	-8
95 Oct 17	core	1.24	0	...	0.12	0.7	50
	C6	0.36	0.30	-86	0.35	1.0	...
	C5	0.18	1.13	-98	1.08	1.0	...
95 Dec 12	core	1.92	0	...	0.11	0.8	-50
	C6	0.24	0.36	-97	0.25	0.8	-56
	C5	0.28	1.30	-90	1.30	0.9	-86
96 Mar 05	core	1.18	0	...	0.17	0.8	-73
	C6	0.24	0.43	-89	0.35	0.9	-10
	C5	0.12	1.35	-99	1.13	0.9	60
96 Mar 26	core	0.95	0	...	0.17	0.7	-70
	C6	0.35	0.38	-95	0.38	0.9	-1
	C5	0.13	1.33	-108	1.20	0.8	3
96 Apr 02	core	1.12	0	...	0.17	0.8	-75
	C6	0.30	0.42	-90	0.25	0.7	50
	C5	0.03	1.39	-100	1.12	0.6	10
96 Apr 24	core	0.92	0	...	0.15	0.8	0
	C6	0.24	0.59	-90	0.43	0.8	-80
	C5	0.05	1.42	-99	1.49	0.8	-63
96 Aug 20	core	1.06	0	...	0.12	0.7	80
	C6	0.45	0.70	-89	0.50	0.8	85
96 Sep 03	core	0.93	0	...	0.12	0.8	81
	C6	0.42	0.73	-95	0.42	0.7	-66
96 Sep 17	core	1.03	0	...	0.15	0.7	62
	C6	0.35	0.78	-92	0.43	0.8	84
96 Sep 19	core	0.91	0	...	0.17	0.7	3
	C6	0.33	0.80	-92	0.40	0.8	80
96 Oct 01	core	1.24	0	...	0.18	0.8	18
	C6	0.32	0.79	-86	0.40	0.7	56

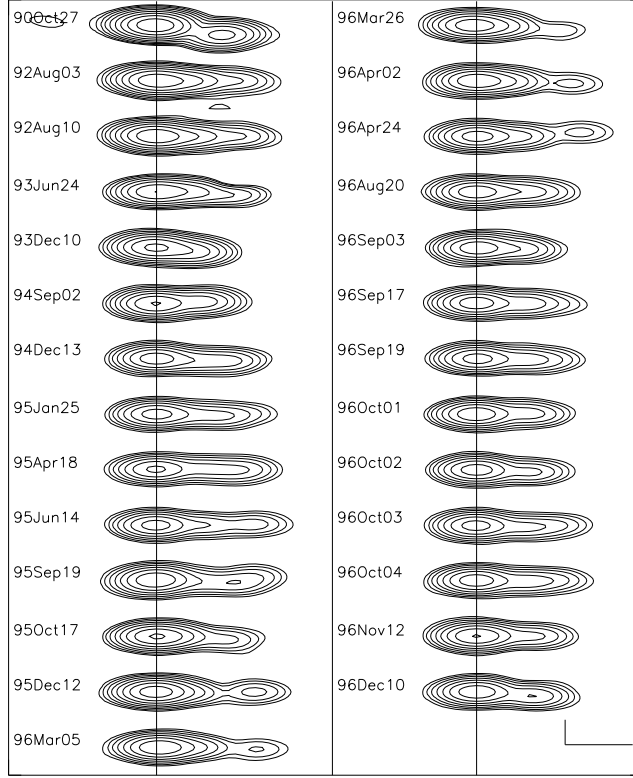


FIG. 1.— 8 GHz VLBI maps of OJ 287. Contour levels increase as 2^n . The lowest contour level is $0.01 \text{ Jy beam}^{-1}$, corresponding to $n = 0$. The restored circular beam is 0.6 mas. The stationary component (the VLBI core) is on the east side (left), while the moving components are to the west (right). The tick in the lower part of the map indicates the size in mas. Note that the maps are stretched in right ascension.

TABLE 2—CONTINUED
MODEL FITS TO OJ 287 AT 8 GHz.

Epoch	Comp.	Flux [Jy]	r [mas]	PA ^a [°]	θ^b [mas]	AR ^c	PA ^d [°]
96 Oct 02	core	0.99	0	...	0.17	0.8	-12
	C6	0.27	0.82	-96	0.48	0.6	-59
96 Oct 03	core	0.89	0	...	0.16	0.8	-18
	C6	0.43	0.84	-97	0.85	0.7	-80
96 Oct 04	core	1.03	0	...	0.16	0.8	-6
	C6	0.37	0.84	-92	0.50	0.8	-85
96 Nov 12	core	1.41	0	...	0.17	0.8	20
	C6	0.43	0.87	-91	0.66	0.6	84
96 Dec 10	core	1.16	0	...	0.18	0.8	-135
	C6	0.49	0.86	-98	0.50	0.6	70

^aPosition angle of the component.

^bMajor axis of the elliptical component.

^cAxial ratio of the elliptical component.

^dPosition angle of the major axis of the elliptical component.

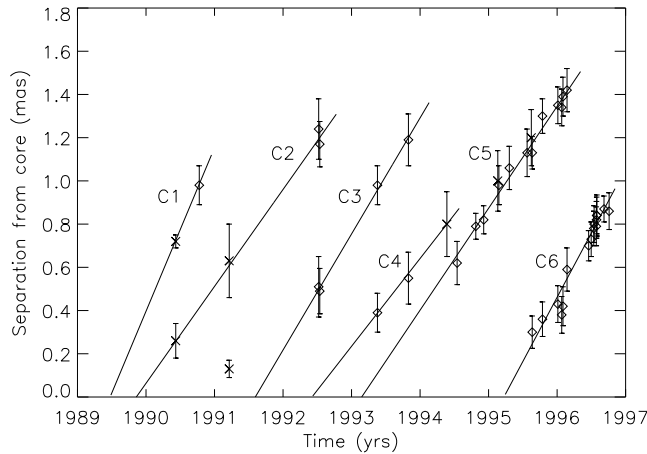


FIG. 2.— Motion of components in OJ 287. The vertical axis shows the separation in mas of the center of the component from the core. The straight lines provide estimates of the presumed zero separation of components C1 to C6 under the assumption of rectilinear motion at constant velocity. The symbol \diamond corresponds to our data and \times to published data. At 1990.47 is 8 GHz data from Gabuzda & Cawthorne (1996), at 1991.27 43 GHz data from Tateyama et al. (1996), at 1994.52 8 GHz data from Fey et al. (1996), and at 1995.28 and 1995.77 8 GHz data from Fey & Charlot (1997). The error bars on component positions are assumed to be one-eighth of the beamwidth.

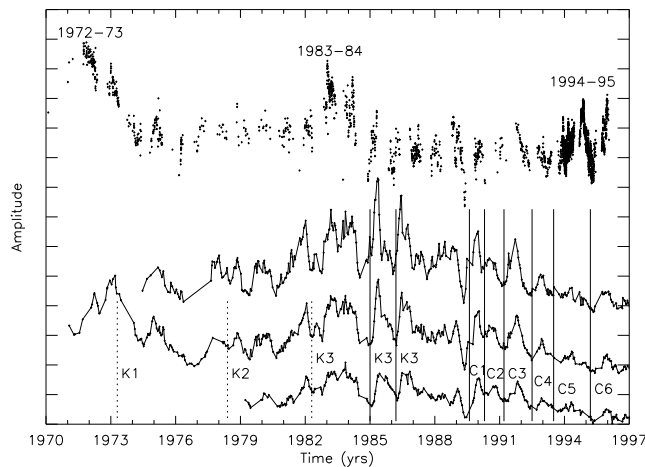


FIG. 3.— Optical and radio light curves of OJ 287. The optical data are from Figure 2 of Sillanpää et al. (1996). The radio data are from the University of Michigan Radio Astronomy Observatory. From top to bottom the plot shows: V-band optical data, and 15 GHz, 8 GHz, and 5 GHz radio data. Each tick mark on the ordinate corresponds to a flux density of 2 Jy for the radio data, and an amplitude of 1 magnitude for the optical data. The vertical lines indicate the beginning of the outburst related to each VLBI component. The dashed lines indicate the epochs of the birth of components K1, K2, and K3. The multiple lines shown for component K3 are discussed in the text. The epochs of double-peaked optical outbursts are indicated over each such outburst.

to zero separation agrees well with the start of the radio outburst at 1989.5. Component C3 would be related to the outburst that started in 1991.5. There is also a weak knot observed near the core in 1991.27 at 43 GHz, which may either be component C3 itself or another component. The radio light curve shows a substructure which may be linked with this component, suggesting that it might have been an intrinsically weak or short-lived component, and faded or merged with C3. Component C4 has 3 data points; the farthest point from the core is a measurement obtained from VLBA data (Fey, Clegg, & Fomalont 1996). This component is associated with a single radio outburst that started in 1992.5. The next component, C5, has the largest separation from the core, and is probably associated with a radio outburst that started in 1993.4. Two points from VLBA data at 8 GHz (Fey & Charlot 1997) have been included in the curve. The small separation between C4 and C5 raises the question of whether or not they can be regarded as one component. In the one radio outburst

per VLBI component scheme, C4 and C5 are individual components which merge later into C5. One weak point to this interpretation is the non-detection of C5 closer to the core in the 1993 December data. However, it could be too close to C4 to be discernible as a separate component at this time. If C4 and C5 are separate components, we would expect a merging of these two components around the end of 1994. In fact, an increase in the flux density of component C5 in 1994 December could be taken as an indication of such an event. Finally, component C6 could be related to the outburst that started in 1995.4.

We have also examined a series of geodetic VLBI maps at 8 GHz obtained by Vicente et al. (1996). They have interpreted the structure of OJ 287 in terms of helical motion, with an indication of a small loop at a distance of about 0.6 mas from the core. They claim a second loop at 2.4 mas is consistent with VLBI data at 5 GHz (Roberts et al. 1987; Gabuzda et al. 1989). Even so, they found no evidence of boosting of K3 as would be expected from the

geometrical effects of a helically moving feature, and the positions of K2 appeared well below the calculated helical trajectory. Even revising the K2 positions upwards (Vicente et al. 1996), the fit does not improve much. Now, if we are allowed to break the component corresponding to epoch 1986.81 (Figure 3 of Vicente et al. 1996) into 2 subcomponents at 0.4 and 0.8 mas, a resolution of 0.5 mas would hardly distinguish between the two models. We could then have rectilinear motion for both components with a proper motion of about 0.4 mas yr^{-1} . An appealing support for the two rectilinear components is the existence of well-defined radio outbursts corresponding to their estimated zero-separation epochs, as shown on Figure 3.

We have also looked for VLBI/radio-outburst correlations for the older VLBI components K1, K2, and K3 (Roberts et al. 1987). The derived proper motion for these components ($0.20 - 0.28 \text{ mas yr}^{-1}$) is about twice as low as our measured proper motion. This indicates that, in the past, different components may have been regarded as the same component. The imbalance between the number of knots and the number of radio outbursts is also noticeable on Figure 3. There are at least 2 well-defined radio outbursts between the one related to the birth of K2 in 1978.4 and K3 in 1982.3 (Roberts et al. 1987). A similar occurrence is also present for component K1, indicating that VLBI components may have been missed.

4.2. Optical Light Curve

On the top part of Figure 3 is the optical light curve from Sillanpää et al. (1996). There is a remarkable similarity between it and the radio light curves. Despite the complexity of the structures, most features can be found in both emission bands. The most easily recognizable correlated radio-optical feature is the double structure that occurred in 1983-84, which had a similar amplitude in the radio and in the optical. The double outbursts of 1971-73 and 1994-95 present a pair of almost identical optical flares, while in the radio these features appear almost as single outbursts coincident with the second optical flare. However, upon more detailed inspection, small protrusions on the radio light curves coincident with the first flare of the double peak are also present in 1971 and 1994. Even weak optical-radio substructures can be pinpointed in the feature beginning in 1994. This can be seen in Figure 4, which shows an expanded section of the light curve corresponding to the period of VLBI observations (1990 to 1997). It is also clear that radio features are delayed by a few months relative to optical features. The inclined dashed lines on the figure correspond to a delay of 0.14 yr. The smoother profile at lower frequencies and the time delay between optical and radio bands gives strong support for the synchrotron self-absorption process (Melnikov 1998). We propose that radio-optical structures are self-absorbed synchrotron sources, and the absence of radio features not correlated with optical features may be due to a more compact synchrotron source.

4.3. VLBI Light Curves

Provided that radio and optical emission are synchrotron, it remains to be seen whether this emission originates in the core, the jet or the accretion disk. The high density time coverage offered by the geodetic VLBI observations, particularly for components C5 and C6, enabled

us to study the evolution of the flux of the VLBI components (core and moving components) with time as shown on Figure 4 along with the radio light curves. It is clear that the time variation of the flux of the core follows closely the shape of the radio light curves, while the flux of the moving components remains nearly constant with time. With less data, similar results can be seen for C4 in December 93. The same behavior can also be seen in geodetic VLBI data studied by Vicente et al. (1996), as shown in Figure 5. Another aspect of the flux of the moving components is that it does not depend on the strength of the radio outbursts. For instance, a radio outburst peaking at 7 Jy (K3 of Vicente et al. 1996) has an associated moving component with a flux similar to those associated with outbursts peaking at 2 Jy (e.g., C6 of present work). These results seem to indicate that the VLBI components contribute to the profile of the radio light curve only when they are just emerging from the core at the time of a radio outburst, and are still merged with the core at the resolution of these VLBI observations.

4.4. Binary Systems

We may speculate that the flares are related to an increase in the accretion rate being induced by the passage of the companion mass (Sillanpää et al. 1988). We assume that the synchrotron emission is optically thin at optical bands and self absorbed at radio bands. The absence of radio outbursts coincident with the first peak of the double-peaked optical outbursts could be an indication of a more compact synchrotron source. We also assume that the major flux variations come from the core. Keeping in mind a synchrotron emission mechanism for optical and radio outbursts; and knowing that radio outbursts have irregular periods of about a year while major optical flares appear every 12 years, we may conceive a binary model where the roughly annual outbursts of the core-jet system of the primary are visited every 12 years by the secondary, increasing the flux of the outbursts.

A narrow jet placed on the disk axis of either the coplanar binary model of Sillanpää et al. (1988) or the steep inclined orbit model of Lehto & Valtonen (1996) would provide an appropriate scenario to explain the observed evolution of the VLBI components as well as the radio and optical outbursts. Lehto & Valtonen (1996) have already suggested a narrow cone on the disk axis to explain a sudden fading “eclipse” caused by the secondary passing over the line of sight. However, those binary systems based on the sweeping beam models of Villata et al. (1996) and Katz (1997) would be discarded because they would not account for the observed evolution of the VLBI components and the number of radio outbursts. While a binary system through its accretion disk increases the accretion rate at evenly spaced intervals, the non-periodic nature of nonthermal outbursts would spread the exact timing of the observable effects of this increased accretion rate. This is indeed in accordance with the small variation observed around the period of 12 years. It would also be possible, depending on the duration of the increased accretion rate and the timing of the irregular ejection rate, to observe a flare with a triple structure as reported by Sundelius et al. (1997).

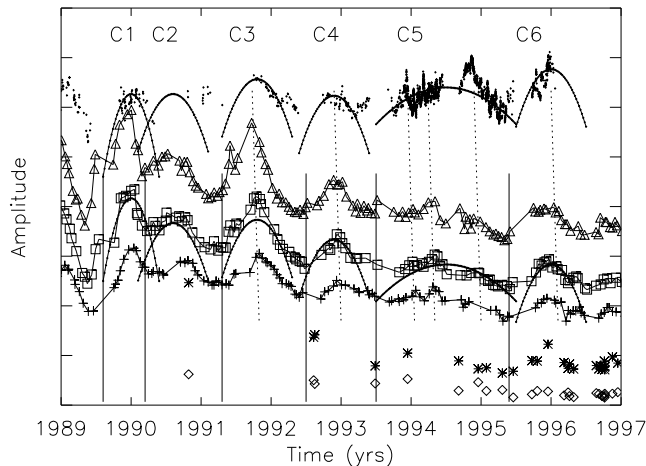


FIG. 4.— Optical, radio, and VLBI light curves. The “arcs” represent the size and shape of the outburst associated with each VLBI component. They are plotted on the optical and 8 GHz data. Below the radio light curves the flux of the core (*) and the sum of the flux of the jet components (\diamond) are also shown. Except for the optical data, the relative amplitudes are all on the same scale. Each tick mark on the ordinate corresponds to a flux density of 2 Jy for the radio data, and an amplitude of 2 magnitudes for the optical data.

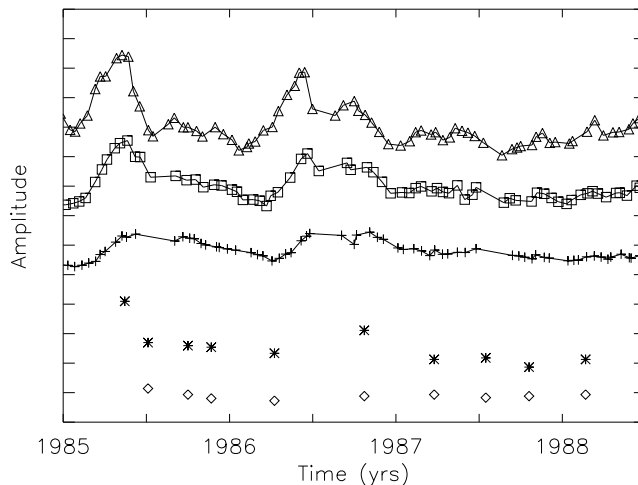


FIG. 5.— Radio light curves compared to VLBI light curves from Vicente et al. (1996). Below the radio light curves are the flux of the core (*) and the sum of the flux of the jet components (\diamond) from Vicente et al. (1996). All amplitudes are on the same scale. Each tick mark on the ordinate corresponds to a flux density of 2 Jy.

5. CONCLUSIONS

We have presented 27 geodetic VLBI maps obtained from the Washington VLBI Correlator Facility at the U.S. Naval Observatory. These maps showed a sequence of 6 VLBI components associated with radio outbursts. The proper motion of the components was found to be around 0.5 mas yr^{-1} , which is almost twice as high as that seen in previous VLBI observations of this source. Such a higher proper motion, along with the larger number of VLBI components, implied a higher component ejection rate for OJ 287, a result supported by the close relationship between the radio outbursts and the appearance of VLBI components.

We have assumed that the radio-optical outbursts are synchrotron emission. The increase in the accretion rate due to the pericenter passage of the companion mass would not directly produce a VLBI component or radio outburst, but would rather provide a means to energize the system and increase the flux of the synchrotron emission. The irregular appearance of radio outbursts/VLBI components

(about once a year), which is intrinsic to the engine, operates continuously. Every 12 years the system is more apt to produce a higher flux; however, the ejection rate of VLBI components and hence the number of radio outbursts is not affected by this process.

C.E.T. thanks the grant received from FAPESP - Fundação de Amparo a Pesquisa do Estado de São Paulo (proc. n. 96/6267-1) to undertake 3 months of work with geodetic VLBI data at USNO (U.S. Naval Observatory). We also thank Aimo Sillanpää for supplying the optical data and the referee for his suggestions and comments which helped with the improvement of the paper. The University of Michigan Radio Astronomy Observatory is supported by the National Science Foundation and by funds from the University of Michigan. The Fortaleza VLBI facility was built and is operated with partial support from U.S. NASA, USNO and NOAA, Brazil ministry of Science and Technology, MCT-FINEP, Mackenzie, INPE and CRAAE (joint center between Mackenzie, INPE, USP and UNICAMP, Brazil).

REFERENCES

- Britzen, S., Witzel, A., Gontier, A.M., Schalinski, C.J., & Campbell, J. 1994, in IAU Symp. 159, Multi-Wavelength Continuum Emission of AGN, ed. T.J.L. Courvosier and A. Blecha (Dordrecht:Kulwer), 423
- Carter, W.E., Robertson, D.S., & MacKay, J.R. 1985, *J. Geophys. Res.*, 90, 4577
- Charlot, P. 1990, *A&A*, 229, 51
- Coates, R.J., Frey, H., Mead, G.D., & Bosworth, J.M. 1985, *IEEE Trans. Geosci. Remote Sensing*, GE-23, 360
- Eubanks, T.M., et al. 1991, in IERS Technical Note No. 8 (IERS:Paris), 73.
- Gabuzda, D.C., & Cawthorne, T.V. 1996, *MNRAS*, 283, 759
- Fey, A.F., Clegg, A.W., & Fomalont, E.B. 1996, *ApJS*, 105, 299
- Fey, A.F., & Charlot, P. 1997, *ApJS*, 111, 95
- Gabuzda, D.C., Wardle, J.F.C., & Roberts, D.H. 1989, *ApJ*, 336, L59
- Guoquiang, T., Rönnäng, B., & Bääth, L. 1987, *A&A*, 185, 87
- Hutchings, J.B., Crampton, D., Campbell, B., Duncan, D., & Glendenning, B. 1984, *ApJS*, 55, 319
- Katz, J.I. 1997, *ApJ*, 478, 527
- Kinman, T.D. 1975, in Variable star and stellar evolution, IAU Symp. 67, ed V.E. Sherwood, & L. Plaut, (Dordrecht: D. Reidel), 573.
- Lehto, H.J., & Valtonen, M.J. 1996, *ApJ*, 460, 207
- Melnikov, V., & Magun, A. 1998, in CESRA - Workshop on coronal explosive events (Finland, 9-13 June, 1998), Metsahovi Publications on Radio Science, 54
- Miller, J.S., French, H.B., & Hawley, S.A. 1978, in Pittsburgh Conference on BL Lac Objects, ed. A. M. Wolfe (Pittsburgh: University of Pittsburgh), 176.
- Pearson, T.J. & Readhead, A.C.S. 1984, *ARA&A*, 22, 97
- Piner, B.G., & Kingham, K.A., 1998, *ApJ*, 507, 706
- Roberts, D.H., Gabuzda, D.C., & Wardle, J.F.C. 1987, *ApJ*, 323, 536
- Rogers, A.E.E., et al. 1983, *Science*, 219, 51
- Sillanpää, A., Haarala, S., Valtonen, M.J., Sundelius, B., & Byrd, G.G. 1988, *ApJ*, 325, 628
- Sillanpää, A., et al. 1996, *A&A*, 315, L13
- Sitko, M.L., & Junkkarinen, V.T. 1985, *PASP*, 97, 1158
- Smith, D.E., & Turcotte, D.L. ed. 1993, *Geodynamics Series 23, Contributions of Space Geodesy to Geodynamics: Crustal Dynamics* (Washington, DC: AGU)
- Sundelius, B., Wahde, M., Lehto, H.J., & Valtonen, M.J. 1997, *ApJ*, 484, 180
- Tateyama, C.E., et al. 1996, *PASJ*, 48, 37
- Tateyama, C.E., Kingham, K.A., Kaufmann, P., Piner, B. G., de Lucena, A.M.P., & Botti, L.C.L. 1998, *ApJ*, 500, 810
- Usher, P.D., 1979, *AJ*, 84, 1253
- Valtaoja, L., Sillanpää, A., & Valtaoja, I., 1987, *A&A*, 184, 57
- Vicente, L., Charlot, P., & Sol, H. 1996, *A&A*, 312, 727
- Villata, M., Raiteri, C.M., Silanpää, A., & Takalo, L.O. 1998, *MNRAS*, 293, L13